VERSITA

CELLULAR & MOLECULAR BIOLOGY LETTERS
http://www.cmbl.org.pl

Received: 27 June 2012
Final form accepted: 20 February 2013
Published online: March 2013

Volume 18 (2013) pp 187-199
DOI: 10.2478/s11658-013-0082-3

Short communication

THE ROLE OF PASSIVE CALCIUM INFLUX THROUGH THE CELL MEMBRANE IN GALVANOTAXIS

PRZEMYSŁAW BORYS*
Department of Chemistry, Silesian University of Technology, ks. M. Strzody 9, 44-100 Gliwice, Poland

Abstract: Passive calcium influx is one of the theories to explain the cathodal galvanotaxis of cells that utilize the electric field to guide their motion. When exposed to an electric field, the intracellular fluid becomes polarized, leading to positive charge accumulation on the cathodal side and negative charge accumulation on the anodal side. The negative charge on the anodal side attracts extracellular calcium ions, increasing the anodal calcium concentration, which is supposed to decrease the mobile properties of this side. Unfortunately, this model does not capture the Ca^{2+} dynamics after its presentation to the intracellular fluid. The ions cannot permanently accumulate on the anodal side because that would build a potential drop across the cytoplasm leading to an ionic current, which would carry positive ions (not only Ca^{2+}) from the anodal to the cathodal part through the cytoplasm. If the cytoplasmic conductance for Ca^{2+} is low enough compared to the membrane conductance, the theory could correctly predict the actual behavior. If the ions move through the cytoplasm at a faster rate, compensating for the passive influx, this theory may fail. This paper contains a discussion of the regimes of validity for this theory.

Key words: Galvanotaxis, Electrotaxis, Passive influx, Leak current, PNP equation, Electrodiffusion, Motility

* Author for correspondence. e-mail: Przemyslaw.Borys@polsl.pl; tel/fax: +48 32 237-17-22

Abbreviations used: PMCA – plasma membrane Ca^{2+} ATPase; PNP equation – Poisson-Nernst-Planck equation; SERCA – sarco/endoplasmic reticulum Ca^{2+} ATPase; TRPC – transient receptor potential cation channels; VGCC – voltage-gated calcium channel

INTRODUCTION

Cellular motility refers to the phenomena of cellular migration, which are involved in many biological processes. Among other things, they are essential for wound healing, organ and tissue formation in morphogenesis, the immunological response, and sperm cell and bacterial movement [1, 2]. Galvanotaxis is a special class of the motility processes which is guided by external electric fields [3, 4], unlike the other common types of guided migration, such as chemotaxis, which is driven by chemical compound gradients [5] or phototaxis, which is driven by light intensity [6].

The physiological (directed current) electric fields for galvanotaxis are mainly produced in the epithelial tissues, where a transepithelial potential is generated due to the polar structure of the epithelilal cells [7-10]. The apical and basolateral membranes of such cells contain unequal amounts of the Na^+ and K^+ channels and the Na^+-K^+-ATP-ases: the apical part contains the Na^+ channels, while the basolateral part contains the K^+ channels and the Na^+-K^+-ATP-ases. This arrangement causes the Na^+ ions to flow through the epithelia from the apical side to the basolateral side. The ionic current flowing into the basolateral region raises the potential of this part until the backward current through the paracellular pathway becomes equal to the incoming current [8, 9].

The role of epithelial cells in the generation of endogenous potentials suggests that galvanotactic processes take place in organs and glands that are surrounded by layers of such cells. They are also important during embryogenesis [10]. Probably the most recognizable example of galvanotactic process can be seen in the healing of a cut epithelium, where the wound creates a shortcut between the apical and basolateral layer, leading to a potential gradient along the epithelium surface which drives the epithelilal cells to move towards the cathode to close the wound. Other important examples of galvanotaxis appear in the neurulation of amphibians or in angiogenesis [9]. Galvanotaxis could also be involved in the invasiveness of metastatic cancer cells, as shown for rat prostate cancer, where the metastatic cells exhibit cathodal galvanotaxis [4]. A scenario has been proposed where cathodal migration forces the metastatic cells to move into the lumen of the epithelial ducts (to become detectable in semen or urine) until the deformation of the epithelium results in a loss of transepithelial potential, which allows invasion of the surrounding tissue [4, 10]. More examples of galvanotaxis can be found in [8-10].

The cell migration in galvanotaxis can take one of two possible directions: cathodal or anodal. Cathodal galvanotaxis is more prevalent (e.g. bovine corneal epithelial cells, bovine aortic vascular endothelial cells, human retinal pigment epithelial cells, human keratinocytes, amphibian neural crest cells, fish epidermal cells and metastatic rat prostate cells [10]), but there exist cases of anodal behavior, for example weakly metastatic rat prostate cancer cells, human granulocytes, human vascular endothelial cells and metastatic human breast cancer cells [10]. Some cells even exhibit a combined mode of operation, with

the migration direction dependent on the environmental conditions. An example of such a system is formed by the peripheral lens epithelial cells, which choose a direction depending upon the field strength [8].

The galvanotactic responses are typically explained using two overlapping classes of mechanisms. The first class involves the electrically induced reorientation of the membrane receptors for the growth factors, while the second class involves internal perturbations in calcium distribution [8]. The first class delivers two options to drive the receptor reorientation. First, it is possible to consider the electrophoresis of negative proteins in the cytoplasm under the action of an external electric field, which leads to their accumulation on the anodal side. Second, it is possible to consider electroosmosis, which overcomes the electrophoretic effect due to the cathodal drag of water, driven by positive cations [8]. This option results in a cathodal accumulation of the receptors and supports a more general picture of cathodal galvanotaxis. Galvanotaxis based on receptor rearrangement requires some time to reach the stationary galvanotactic response, which is typically less than ten minutes [9].

Another class of mechanisms highlights the importance of calcium ions for the cellular growth and motility processes [11]. They promote the capping of the barbed ends of actin filaments by gelsolin, preventing polymerization, and they cause myosin contraction, which is one of the factors responsible for the detachment of the rear side of the cell from the surface in a motile process [6, 10]. In this model, the variations of the calcium influx over various parts of the cell membrane may regulate the directional movements of cells. The calcium influx for galvanotaxis may be of various origin. In some cases, it can be activated by the voltage-gated calcium channels (VGCCs) or stretch-activated calcium channels, as was suggested for human keratinocytes and green paramecia in [12, 13]. It could be also mediated by the TRPC channels, which may be relevant for chemotaxis [14, 15]. In other cases, when cells are not equipped with calcium channels, it can be of a passive nature [4, 10]. The galvanotactic response in such a mode can rise in less than 30 seconds [4].

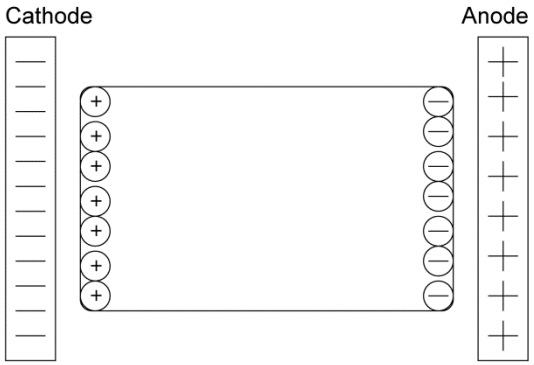

Fig. 1. The polarization of ions within the cell in the presence of an externally applied electric field.

The role of the passive calcium influx was originally presented in [16], a supporting picture of the calcium dynamics was proposed in [17], and the whole theory was summarized in [18]. It was stated that the intracellular fluid in an external electric field becomes polarized so that the cations become attracted to the negative electrode (cathode), leaving anions on the anodal side (Fig. 1). The negative charge on the anodal side attracts the extracellular calcium ions into the cell, increasing the anodal concentration and inhibiting the anodal growth of the actin filaments, resulting in cathodal galvanotaxis.

This theory is still in use to explain current research results [3, 10, 19-21] but it has yet to be investigated in depth from a theoretical point of view. One striking question that is raised by the theory is why the calcium ions should accumulate on the anodal end of the cell if this region is in general depleted of positive charges (Fig. 1). The detailed analysis presented here answers this question and shows cases where the accumulation does not occur. The effect depends on the relationship between the cytoplasmic electrical conductance for the Ca^{2+} ions (expressed by the diffusion coefficients) and the electrical conductance of the membrane. If the passive influx is small compared to the resulting cytoplasmic current, the accumulation does not occur. However, if the Ca^{2+} influx is large, e.g. due to leakage channels, the cytoplasmic current cannot catch up with the ion removal, and accumulation occurs until a potential difference builds up to increase the cytoplasmic current sufficiently.

METHODS

The cell is modeled by an one-dimensional Poisson-Nernst-Planck equation, i.e. a Nernst-Planck equation describing the diffusion of ions supplemented by the Poisson equation to obtain the electrical field distribution produced by the ions. The derivation of this equation set is shown in details in [21] and the final form is [21-24]:

$$\frac{\partial c_i}{\partial t} = \frac{\partial}{\partial x} D_i \left[\frac{\partial c_i}{\partial x} + \frac{z_i F c_i}{RT} \frac{d\varphi}{dx} \right]$$
$$\frac{d^2\varphi}{dx^2} = -\sum \frac{z_i F c_i}{\varepsilon} \qquad (1)$$

where c_i is the concentration of the i-th ionic species; t is the time; x is the position coordinate; D_i is the diffusion coefficient of the i-th ionic species; z_i is the multiplicity of elementary charge associated with the i-th ionic species; R is the gas constant (R = 8.314 J mol^{-1} K^{-1}); T is the temperature (T = 300 K); F is Faraday's constant (F = 96485.3415 C mol^{-1}); φ is the electric potential; and ε is the electrical permittivity of the cytoplasm, which is set close to the value for water (ε = 10^{-9} F m^{-1}).

As can be seen, the Nerst-Planck equation (the first equation in (1)), is a diffusion equation that takes into account the external force originating from

the electric potential gradient (from the electric field). The derivation is straightforward after consideration of fluxes driven by the diffusion process and by the external force, which imposes a "drift velocity" when balanced by the friction force [21]. Each time the charge distribution changes after evaluation of the Nernst-Planck equation, the resulting electric potential distribution (the force field) must be recalculated by the Poisson equation (the second equation in (1)). The differential equations are solved in a similar way as was done in [21], using the explicit upwind scheme by the finite difference method with lattice spacing equal to 125 nm [18, 25]. The diffusion coefficients for the intracellular ions are taken according to the literature and are presented in Table 1. The intracellular concentrations are shown in Table 2 (after [29]).

Table 1. Diffusion coefficients of the intracellular ions.

Ion	Diffusion coefficient
Na^+	1.23×10^{-10} m^2s^{-1} [26]
K^+	17.3×10^{-10} m^2s^{-1} [27]
Ca^{2+}	5.3×10^{-10} m^2s^{-1} [28]

Table 2. The intracellular concentrations of the ions.

Ion	Intracellular concentration [mM]
Na^+	12
K^+	139
Ca^{2+}	< 0.0002

These ionic concentrations are supplemented by the concentration of anionic proteins (138 mM) and HCO_3^- (12 mM). For simplicity, only the Na^+, K^+, Ca^{2+} ions and the immobile proteins are considered here. The concentrations of the latter are adjusted to provide a net internal charge consistent with the membrane potential of -90 mV. This charge results from the membrane capacitance by $Q = CU$ with the membrane capacitance per unit surface equal to $C_m = 10^{-9}$ F m^{-2} [30]. The boundary conditions for the Nernst-Planck equation were set to a reflecting type. For the Poisson equation, the left boundary condition was set to match the electric field imposed on the membrane, i.e. the membrane potential (90 mV supplemented with the contribution of the external DC field) divided by the membrane thickness (equal to 7 nm). The right boundary condition of the Poisson equation was set to 0 mV to set a reference potential. The Poisson equation cannot have two Neumann conditions because the solution could be found only up to an additive constant and the electric field on the second boundary is not arbitrary, but is determined by the total charge located within the cell and by the left boundary condition. Imposing the electrical field on the left boundary, one should keep in mind that the electrical permittivity of the

cytoplasm (assumed as 10^{-9} F m^{-1}) is approximately 14 times larger than that of the cell membrane (as estimated from C_m in a flat capacitor model). This weakens the magnitude of the field on the boundary compared to the field within the cell membrane.

To model the passive fluxes and pump operation, their contributions are injected at each time step for x = 0 (the cathodal side of the cell) and x = L (the anodal side of the cell) in a proportion which results from the expected current flow, $\Delta Q = I\Delta t$. The passive ionic flow is introduced based on [31], with passive conductances equal to g_{Na} = 0.2 Sm^{-2}, g_K = 0.7 Sm^{-2} and the corresponding Nernst potentials equal to E_{na} = 71 mV, E_K = -97 mV. The current through the membrane is then calculated by:

$$I_i = g_i\left(U - E_i\right) \tag{2}$$

where I_i is the current of i-th ion; g_i and E_i are the membrane conductance and the Nernst potential of the i-th ion, respectively; and U is the membrane potential. The action of the Na-K-ATP-ase is modeled after [31] by the following equation set:

$$\begin{aligned} I_K &= -2I_{max}A_{pump} \\ I_{Na} &= 3I_{max}A_{pump} \\ A_{pump} &= \left(1+\frac{K_{mK}}{[K]_o}\right)^{-2}\left(1+\frac{K_{mNa}}{[Na]_i}\right)^{-3} \end{aligned} \tag{3}$$

where I_{max} = 130 mA m^{-2}; K_{mK} = 3.5 mM l^{-1}; and K_{mNa} = 10 mM l^{-1}. The subindex "o" denotes the environment "outside" the cell, while "i" means "inside" the cell.

The membrane conductance for the calcium ions was estimated in the Nernst potential framework, considering the extracellular $[Ca^{2+}]$ concentration to be equal to 1.8 mM [29]. This results in a value of E_{Ca} = 117.69 mV. The conductance of the membrane is difficult to estimate, but there are several sources. First, after [32], the permeability of the lens cell membrane for Ca^{2+} should be in the range (8 x 10^{-15} cm s^{-1}, 2.5 x 10^{-11} cm s^{-1}). Rescaling this to the conductance values for equation (2) results in a g_{Ca} contained in the range (132 pS m^{-2}, 412.4 nS m^{-2}). On the other hand, based on [33], one can expect leak calcium currents of magnitude equal to 0.36 pA in A7r5 cells that have a diameter of about 16 μm. Such large currents occur due to the leakage channels and indicate a calcium conductance g_{Ca} = 2.1 mS m^{-2}, which is orders of magnitude larger than for a simple lipid membrane. The reported ranges of variability are investigated in the following simulations.

To complete the model, it is also necessary to consider the membrane regulatory mechanisms for the calcium concentration, i.e. the plasma membrane Ca-ATP-ase (PMCA) pump. It has only one calcium-binding site, unlike SERCA pumps [34]

and therefore, after the threshold concentration for calmodulin activation is obtained, the PMCA current can by modeled by:

$$I_{Ca} = K_{Ca}[Ca]_i \quad (4)$$

where K_{Ca} is a constant set to give the PMCA current equal to the leak current at resting concentration of the internal calcium $[Ca]_i$ close to the membrane.

RESULTS AND DISCUSSION

The first simulation (Fig. 2) concerned a cubic cell with a side length l = 16 μm in an electric field of 6 V/cm. This resulted in a depolarizing contribution on the cathodal membrane side of about 5 mV and a hyperpolarizing contribution on the anodal side (also about 5 mV). Starting with a stationary ionic distribution obtained for a cell with equal potentials on both ends, the external electric field was enabled and the simulation was run for 50 ms to obtain an ionic distribution which is close to the equilibrium, reached at $t \rightarrow \infty$ (about 4 days of computing time per simulation for a 128 node lattice). Because the predicted concentration changes reach at most 0.3% of the bulk concentration, the bulk value of 0.2 μM is subtracted from the presented results.

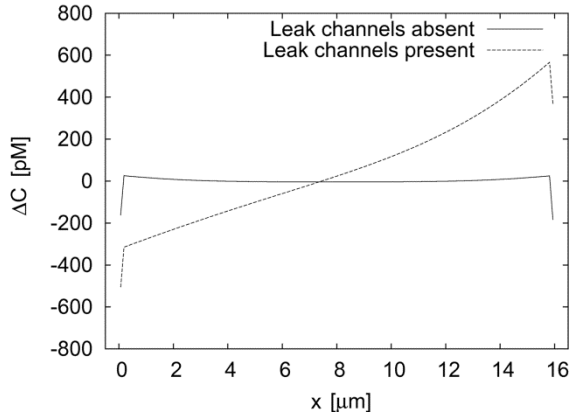

Fig. 2. The equilibrated calcium profile for a cell with leak channels (dashed line) or without them (solid line). The initial bulk intracellular concentration (0.2 μM) is subtracted to show the profile details.

Even without a careful analysis of the results, it can be seen that for $g_{Ca} = 412.4$ nS m^{-2}, the anodal Ca^{2+} accumulation does not occur in the cell. Actually, a depletion occurs, since the anodal side has a calcium concentration that is 183.79 pM lower than the bulk concentration, while the cathodal side has a calcium concentration that is 163.34 pM lower than the bulk, i.e. the anodal part has lower calcium concentration than the cathodal part. However, such an accumulation occurs for $g_{Ca} = 2.1$ mS m^{-2}.

The concentration changes are calculated on a lattice with spacing equal to 125 nm, however the boundary ionic concentration profile is rather expected to spread over the Debye length, which is much shorter and equals to 0.7 nm [21]. To investigate the fine structure of the Ca^{2+} distribution, the calculations were repeated on a lattice with spacing equal to 62.5 nm (a week of computing time per simulation). If there is a Debye layer contribution, the boundary concentration change should multiply by a factor of two because the whole concentration shifts to the compartment that is most adjacent to the membrane, and the width of this compartment decreases by two. If the Debye layer contribution is absent, the concentration should not change. The results are shown in Figs 3 and 4.

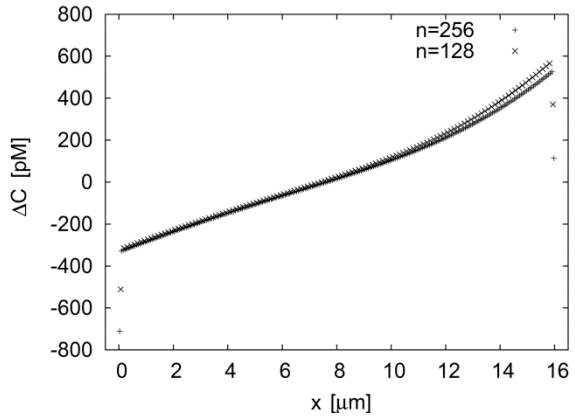

Fig. 3. The change in the concentration profile for g_{Ca} =2.1 mS m^{-2} for a coarse ('x' symbols, n = 128 nodes) and fine ('+' symbols, n = 256 nodes) lattice.

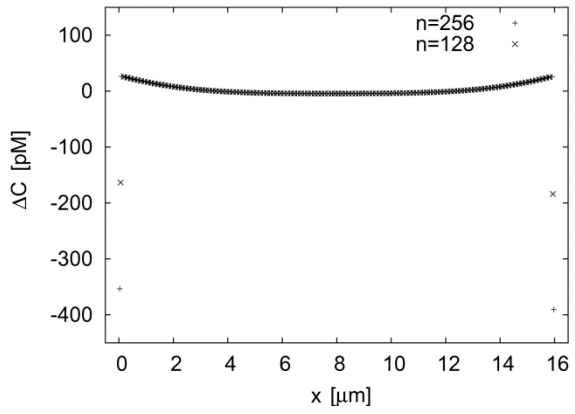

Fig. 4. The concentration change profile for g_{Ca} =412.4 nS m^{-2}. Calculations on a coarse ('x' symbols, n = 128 nodes) and fine ('+' symbols, n = 256 nodes) lattice.

Both figures reveal a twofold change in the concentration with respect to the general trend baseline when moving to a fine lattice. Subtracting the general trend line (linear approximation) from the boundary concentration changes gives the results shown in Table 3.

Table 3. Concentration change on the boundary nodes of the lattice with respect to the bulk concentration.

	x = 0 μm	x = 16 μm
g_{Ca} = 2.1 mS m^{-2}, h = 125 nm	-190.1 pM	-210.3 pM
g_{Ca} = 2.1 mS m^{-2}, h = 62.5 nm	-379.7 pM	-417.7 pM
g_{Ca} = 412.4 nS m^{-2}, h = 125 nm	-190.4 pM	-210.1 pM
g_{Ca} = 412.4 nS m^{-2}, h = 62.5 nm	-380.3 pM	-417.1 pM

In the case of g_{Ca} =2.1 mS m^{-2}, the general trend line differs on the coarse and fine lattices due to a change in the PMCA stimulation because of a different concentration for x = 16 μm. This small discrepancy does not influence the discussion, and optimization of the coefficients would be very difficult, so it is left unchanged. Despite this defect, Table 3 shows that the boundary concentrations on a fine lattice change twofold with respect to the baseline when moving from the coarse to fine lattice estimates. This allows the calculation of the exact Debye layer concentration drop after multiplying the values from the coarse lattice by 125 nm/0.7 nm, which is shown in Table 4.

Table 4. Concentration change in the Debye layer with respect to the bulk concentration.

	x = 0 μm	x = 16 μm
g_{Ca} = 2.1 mS m^{-2}	-33.9 nM	-37.5 nM
g_{Ca} = 412.4 nS m^{-2}	-34 nM	-37.5 nM

It is possible to conclude that the boundary layer contribution does not change in relation to the Ca^{2+} membrane permeability and that the anodal side contains less calcium than the cathodal side. However, the general Ca^{2+} profile changes and this matters for the cortical cytoplasm layer, where actin filaments reside [6]. The boundary concentration changes related to the baseline profile (without Debye layer effects) are shown in Table 5.

Table 5. The boundary concentration change related to the general concentration distribution without consideration of the Debye layer effects.

	x = 0 μm	x = 16 μm
g_{Ca} =2.1 mS m^{-2}	-0.32 nM	0.58 nM
g_{Ca} = 412.4 nS m^{-2}	0.03 nM	0.03 nM

It is interesting to ask whether calcium accumulation occurs in the cortical layer of the cytoplasm or if calcium is removed from this layer. After [6], the reasonable cortical thickness can be assumed equal to 0.5 μm. Performing the simulation with a spatial step set to this value, it is possible to observe the calcium dynamics in the outermost lattice intervals, which represent the cytoplasm cortex. According to such calculations, a cathodal galvanotaxis regime for the inspected cell should occur for $g_{Ca} > 78$ μS m^{-2}. A general chart of the threshold conductance in relation to the cellular diameter is shown in Fig. 5 and takes the form of a power law, $g_{Ca\ threshold} = 20{,}000$ μS $\mu m^2/d^2$. This is a decreasing trend which may be explained for a cubic cell because the membrane conductance grows like d^2 with d (the cell edge size), while the cytoplasm conductance grows slower, like d, because the cross section increment is accompanied with the elongation of the cell. Therefore, for cells that are big enough, the anodal accumulation of Ca^{2+} could take place no matter whether they possess the leakage channels or not.

The presented theory requires validation by experimental procedures, but it seems to have the potential to explain the cathodal galvanotaxis of the highly metastatic Mat-LyLu rat prostate cancer cells in relation to the anodal galvanotaxis of the weakly metastatic AT-2 cells. These cells exhibit a rapid motile reaction to electrical stimulation (beyond 30 seconds), which suggests that it is initially not mediated by the electrophoresis or electroosmosis of any receptors, which respond after several minutes and may take some part in the response on later times [10]. These cells also exhibit no calcium currents and are insensitive to the VGCC blockers (they do not have VGCCs). The theory that could explain their behavior would be the passive calcium influx, but it fails in case of the weakly metastatic cells, which move towards the anode, and would not explain the voltage-gated sodium channel dependency of the highly metastatic cells on galvanotaxis.

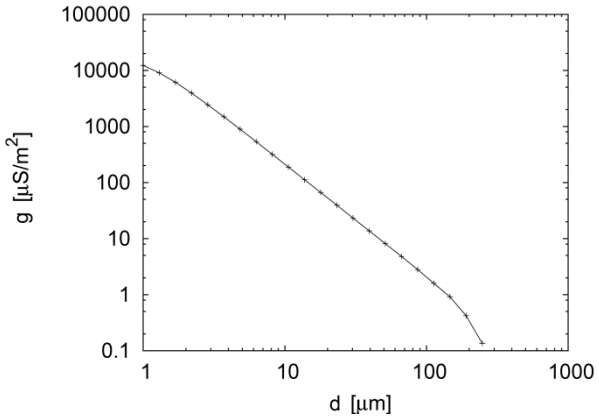

Fig. 5. The dependency of the threshold conductance of the cell membrane on the diameter of the cell. Below the line, the anodal part of the cell becomes depleted of calcium ions, while above the line, it is enriched in calcium ions (fixed voltage change on the membrane).

Taking into account the point of view where the membrane permeability for calcium is not very high, one could understand the anodal behavior of the AT-2 cells, and the cathodal galvanotaxis of the Mat-LyLu cells would stem from the electrostatic repulsion of calcium by the entering sodium ions [4, 21]. Importantly, it seems reasonable to generalize that the galvanotactic effect, due to internal calcium distribution (as in AT-2 cells), should be much smaller than the effects seen in cells that are equipped with calcium channels [4, 8].

CONCLUDING REMARKS

This paper gives a theoretical analysis of the passive calcium influx theory related to galvanotaxis. The results reveal that the cell membrane conductance for the calcium ions is essential for determining the direction of galvanotaxis by this mechanism. If the conductance is too low, the calcium ions do not enter quickly enough to increase calcium concentration, which equilibrates by a flow through the cytoplasm to the cathodal side. Therefore, to save the theory, the Ca^{2+}-permeable leakage channels need to be taken into consideration, especially for small cells.

Because the electrical cytoplasmic conductance for the ions depends on the size of the cell and grows in proportion to d, while the passive membrane current increases in proportion to d^2, the larger cells reveal a smaller conductance threshold for calcium accumulation than the smaller cells.

In general, the modeling confirms the considered theory in some cells and puts constraints on its validity. Additionally, the model may suggest the existence of leakage channels for calcium ions based on the direction of galvanotaxis, provided other galvanotactic factors are excluded.

REFERENCES

1. Ananthakrishnan, R. and Ehrlicher, A. The forces behind cell movement. **Int. J. Biol. Sci.** 3 (2007) 303-317.
2. Korohoda, W., Kucia, M., Wybieralska, E., Wianecka-Skoczeń, M., Waligórska, A., Drukała, J. and Madeja, Z. Solute-dependent activation of cell motility in strongly hypertonic solutions in Dictyostelium discoideum, Human Melanoma HTN-140 cells and Walker 256 Carcinosarcoma cells. **Cell. Mol. Biol. Lett.** 16 (2011) 412-430.
3. Shanley, L.J., Walczysko, P., Bain, M., MacEwan, D.J. and Zhao, M. Influx of extracellular Ca^{2+} is necessary for electrotaxis in Dictyostelium. **J. Cell Sci.** 119 (2006) 4741-4748.
4. Djamgoz, M.B.A. Directional movement of rat prostate cancer cells in direct-current electric field: involvement of voltage-gated Na^+ channel activity. **J. Cell Sci.** 114 (2001) 2697-2705.
5. Alt, W., Deutsch, A. and Dunn, G. **Dynamics of cell and tissue motion.** Birkhauser, Basel, 1997.

6. Bray, D. **Cell movements: from molecules to motility.** 2nd edition, Garland Publishing, New York, 2000.
7. Barnes, F.S. and Greenbaum. B. (Eds). **Handbook of biological effects of electromagnetic fields.** CRC press, Boca Raton, 2007.
8. Nuccitelli, R. A role for endogenous electric fields in wound healing. **Curr. Top. Dev. Biol.** 58 (2003) 1-26.
9. McCaig, C.D., Rajnicek, A.M., Song, B. and Zhao, M. Controlling cell behavior electrically: current views and future potential. **Physiol. Rev.** 85 (2005) 943-978.
10. Mycielska, M.E. and Djamgoz, M.B.A. Cellular mechanisms of direct-current electric field effects: galvanotaxis and metastatic disease. **J. Cell Sci.** 117 (2004) 1631-1639.
11. Fang, K.S., Behnom, F., Nuccitelli, R. and Isseroff, R.R. Migration of human keratinocytes in electric fields requires growth factors and extracellular calcium. **J. Invest. Dermatol.** 111 (1998) 751-756.
12. Trollinger, D.R., Isseroff, R.R. and Nuccitelli, R. Calcium channel blockers inhibit galvanotaxis in human keratinocytes. **J. Cell. Physiol.** 193 (2002) 1-9.
13. Aonuma, M., Kadano, T. and Kawano, T. Inhibition of anodic galvanotaxis of Green Paramecia by T-type calcium channel inhibitors. **Z. Naturforsch.** 62c (2007) 93-102.
14. Wang, G.X. and Poo, M.M. Requirement of TRPC channels in netrin-1-induced chemotropic turning of nerve growth cones. **Nature** 434 (2005) 898-904.
15. Torossian, F., Bisson, A., Vannier, J.P., Boyer, O. and Lamacz, M. TRPC expression in mesenchymal cells. **Cell. Mol. Biol. Lett.** 15 (2010) 600-610.
16. Cooper, M.S. and Keller, R.E. Perpendicular orientation and directional migration of amphibian neural crest cells in dc electrical fields. **Proc. Natl. Acad. Sci. USA** 81 (1984) 160-164.
17. Chen, T.H. and Jaffe, L.F. Effects of membrane potential on calcium fluxes of pelvetia eggs. **Planta** 140 (1978) 63-67.
18. Robinson, K.R. The responses of cells to electrical fields: a review. **J. Cell Biol.** 101 (1985) 2023-2027.
19. Isaacson, B.M. and Bloebaum, R.D. Bone bioelectricity: what have we learned in the past 160 years? **J. Biomed. Mat. Res. A** 95A (2010) 1270-1279.
20. Gao, R.Ch., Zhang, X.D., Sun, Y.H., Kamimura, Y., Mogilner, A., Devreotes, P.N. and Zhao, M. Different roles of membrane potentials in electrotaxis and chemotaxis of Dictyostelium cells. **Eukaryot. Cell** 10 (2011) 1251-1256.
21. Borys, P. On the biophysics of cathodal galvanotaxis in rat prostate cancer cells: Poisson-Nernst-Planck equation approach. **Eur. Biophys. J.** 41 (2012) 527-534.
22. Coalson, R.D. and Kurnikova, M.G. Poisson-Nernst-Planck theory of ion permeation through biological channels. in: **Biological membrane ion**

channels (Chung, S.H., Andersen, O.S. and Krishnamurthy, V. Eds.). Springer, New York, 2007, 449-485.
23. Kurnikova, M.G., Coalson, R.D., Graf, P. and Nitzan, A. A lattice relaxation algorithm for three-dimensional Poisson-Nernst-Planck theory with application to ion transport through the Gramicidin A channel. **Biophys. J.** 76 (1999) 642-656.
24. Rubinstein, I. Electro-diffusion of ions. **SIAM studies in applied mathematics.** Philadelphia, 1990.
25. Ni, M.J., Tao, W.Q. and Wang, S.J. Stability controllable second-order difference scheme for convection term. **J. Therm. Sci.** 7 (1998) 119-130.
26. Abelson, P.H. and Duryee, W.R. Radioactive sodium permeability and exchange in frog eggs. **Biol. Bull.** 96 (1949) 205-217.
27. Hodgkin, A.L. and Keynes, R.D. The mobility and diffusion coefficient of potassium in giant axons from Sepia. **J. Physiol.** 119 (1953) 513-528.
28. Donahue, B.S. and Abercrombie, R.F. Free diffusion coefficient of ionic calcium in cytoplasm. **Cell Calcium** 8 (1987) 437-448.
29. Lodish, H.F., Berk, A., Matsudaira, P., Kaiser C.A., Krieger, M., Scott, M.P., Zipursky, L. and Darnell, J. **Molecular Cell Biology.** Freeman, W.H. New York, 2003.
30. Neher, E. and Sakmann, B. **Single channel recording.** Plenum, New York, 1995.
31. Kager, H., Wasman, W.J. and Somjen, G.G. Simulated seizures and spreading depression in a neuron model incorporating interstitial space and ion concentrations. **J. Neurophysiol.** 84 (2000) 495-512.
32. Zeng, J., Borchman, D. and Paterson, C.A. Calcium permeability in large unilamellar vesicles prepared from bovine lens cortical lipids. **Exp. Eye Res.** 64 (1997) 115-120.
33. Obejero-Paz, C.A., Jones, S.W. and Scarpa, A. Multiple channels mediate calcium leakage in the A7r5 smooth muscle-derived cell line. **Biophys. J.** 32 (1998) 12-21.
34. Di Leva, F., Domi, T., Fedrizzi, L., Lim, D. and Carafoli, E. The plasmamembrane Ca^{2+} ATPase of animal cells: Structure, function and regulation. **Arch. Biochem. Biophys.** 476 (2008) 65-74.